Metabolic response to everolimus in patient-derived triple negative breast cancer xenografts

Leslie R. Euceda[*†], *Deborah K. Hill*[†], *Endre Stokke*[†], *Rana Hatem*[§∥], *Rania El Botty*[⊥], *Ivan Bièche*[§#], *Elisabetta Marangoni*[⊥], *Tone F. Bathen*[†], *Siver A. Moestue*[†▽]

[†] Department of Circulation and Medical Imaging, NTNU, The Norwegian University of Science and Technology, Trondheim, Norway

[§] Institut Curie, PSL Research University, Genetics Department, Paris, France

[∥] Faculty of Pharmacy, Aleppo University, Aleppo, Syria

[⊥] Institut Curie, PSL Research University, Translational Research Department, Paris, France

[#] EA7331, University of Paris Descartes, Paris, France

[▽]Department of Laboratory Medicine, Children's and Women's Health, NTNU, The Norwegian University of Science and Technology, Trondheim, Norway

Corresponding Author: Leslie R. Euceda: leslie.e.wood@ntnu.no

Published in: Journal of Proteome Research, 2017; doi: 10.1021/acs.jproteome.6b00918
http://pubs.acs.org/doi/full/10.1021/acs.jproteome.6b00918

Metabolic response to everolimus in patient-derived triple negative breast cancer xenografts

Leslie R. Euceda[*†], *Deborah K. Hill*[†], *Endre Stokke*[†], *Rana Hatem*[§∥], *Rania El Botty*[⊥], *Ivan Bièche*[§#], *Elisabetta Marangoni*[⊥], *Tone F. Bathen*[†], *Siver A. Moestue*[†▽]

[†] Department of Circulation and Medical Imaging, NTNU, The Norwegian University of Science and Technology, Trondheim, Norway

[§] Institut Curie, PSL Research University, Genetics Department, Paris, France

[∥] Faculty of Pharmacy, Aleppo University, Aleppo, Syria

[⊥] Institut Curie, PSL Research University, Translational Research Department, Paris, France

[#] EA7331, University of Paris Descartes, Paris, France

[▽]Department of Laboratory Medicine, Children's and Women's Health, NTNU, The Norwegian University of Science and Technology, Trondheim, Norway

Keywords: everolimus, HR MAS MRS, metabolomics, mTOR, PI3K pathway, triple negative breast cancer.

ABSTRACT

Patients with triple negative breast cancer (TNBC) are unresponsive to endocrine and anti-HER2 pharmacotherapy, limiting their therapeutic options to chemotherapy. TNBC is frequently associated with abnormalities in the PI3K/AKT/mTOR signaling pathway; drugs targeting this pathway are currently being evaluated in these patients. However, response is variable, partly due to heterogeneity within TNBC, conferring a need to identify biomarkers predicting response and resistance to targeted therapy. In this study, we used a metabolomics approach to assess response to the mTOR inhibitor everolimus in a panel of TNBC patient-derived xenografts (PDX) (n=103 animals). Tumor metabolic profiles were acquired using high-resolution magic angle spinning magnetic resonance spectroscopy. Partial least squares-discriminant analysis on relative metabolite concentrations discriminated treated xenografts from untreated controls with an accuracy of 67% (p=0.003). Multilevel linear mixed-effects models (LMM) indicated reduced glycolytic lactate production and glutaminolysis after treatment, consistent with PI3K/AKT/mTOR pathway inhibition. Although inherent metabolic heterogeneity between different PDX models seemed to hinder prediction of treatment response, the metabolic effects following treatment were more pronounced in responding xenografts compared to non-responders. Additionally, the metabolic information predicted p53 mutation status, which may provide complimentary insight into the interplay between PI3K signaling and other drivers of disease progression.

INTRODUCTION

Pharmacological treatment of breast cancer has progressed notably in the past decades, accounting for much of the improvement in patient survival[1-2]. Currently available systemic treatments include chemotherapy, endocrine therapy, and novel targeted therapies. Chemotherapy has been shown to be the most potent of these treatments[3], but severe adverse effects may limit its use. Endocrine treatment was the first targeted therapy for breast cancer; it is considered to be safe and effective, but is only useful for the treatment of hormone (estrogen and progesterone) receptor positive patients[3]. Novel targeted therapies include the human epidermal growth factor receptor 2 (HER2) inhibitor trastuzumab, which can provide additional benefit to patients overexpressing the cell growth-promoting HER2 (ERBB2) protein[3].

Triple negative breast cancer (TNBC) refers to any breast cancer lacking expression of estrogen receptors (ER), progesterone receptors (PgR), and HER2 protein. These cancers are consequently unresponsive to both endocrine and anti-HER2 therapy, limiting the therapeutic option for these patients to chemotherapy alone. Breast tumor heterogeneity is not only found at the protein level; Perou and Sørlie et al. divided the disease into five naturally-occurring, clinically relevant subtypes based on gene expression[4-5]. TNBC displays a high degree of overlap with the basal-like gene expression subtype, which is associated with the worst prognosis and a high frequency of abnormalities in the phosphatidylinositol-3-kinase (PI3K)/AKT signaling pathway[6-7] (Figure 1). This pathway is involved in cell survival, proliferation, and growth, and has been shown to be deregulated in various human cancers[8].

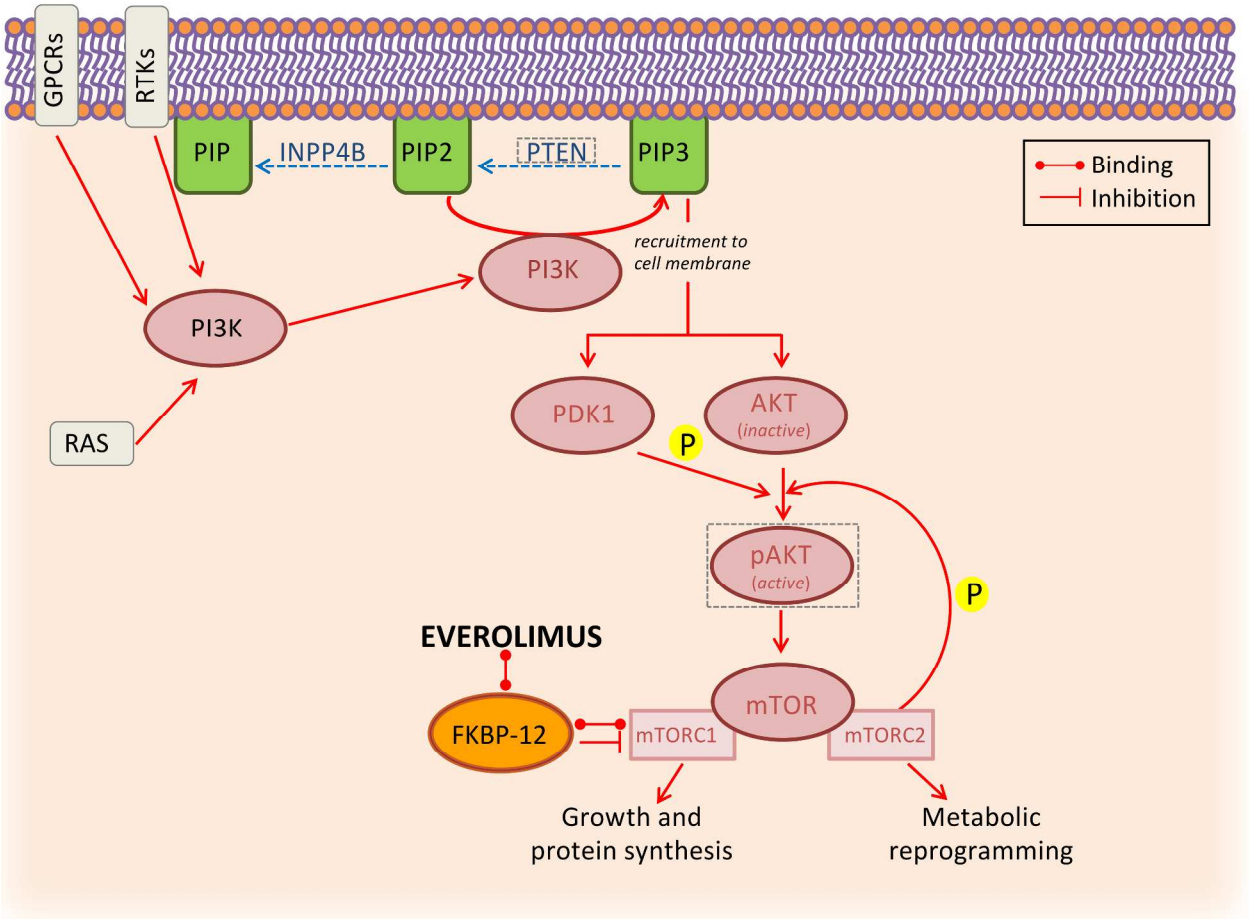

Figure 1. PI3K/AKT signaling pathway in cancer. PI3K can be activated by receptor tyrosine kinases (RTKs), G protein-coupled receptors (GPCRs), and RAS. Activated PI3K phosphorylates phosphatidylinositol 4,5-bisphosphate (PIP2), a plasma membrane phospholipid, and converts it into phosphatidylinositol 3,4,5-trisphosphate (PIP3). PIP3 binds to 3-phosphoinositide dependent protein kinase-1 (PDK1) and AKT, recruiting them to the plasma membrane. This process is negatively regulated by PTEN and INPP4B, which convert PIP3 back to PIP2, and PIP2 back to phosphatidylinositol phosphate (PIP), respectively. Once at the plasma membrane, AKT is activated via phosphorylation by PDK1. Activated AKT then phosphorylates mTOR (mammalian target of rapamycin), which acts as a catalytic subunit in the protein complexes of mTORC1 and mTORC2. mTORC1 is involved in growth and protein synthesis,

while mTORC2 regulates metabolic reprogramming and activates AKT, creating a positive feedback loop. Via association with the FKBP-12 protein, of which mTORC1 is a direct target, everolimus indirectly binds to mTORC1, inhibiting its activity. In the present study, prediction of the expression of the proteins PTEN and pAKT (in gray, dashed boxes) using metabolic data was attempted.

Various inhibitors of the PI3K pathway have been developed for use as cancer therapies. Many of these act upon the mammalian target of rapamycin (mTOR), one of the major effectors downstream of AKT. One such inhibitor is everolimus, a rapamycin analog that binds to the FKBP-12 protein of which mTOR complex 1 (mTORC1) is a direct target[9]. The everolimus-FKBP-12 complex binds to mTORC1, inhibiting further downstream signaling of the PI3K/AKT pathway. Everolimus is approved for treatment of hormone receptor positive[10-11] and HER2 positive[12] breast cancer in combination with hormonal or anti-HER2 therapy, respectively, with the addition of the mTOR inhibitor significantly prolonging progression-free survival (PFS). However, with abnormal PI3K signaling occurring very frequently in TNBC compared to the other breast cancer subtypes, everolimus has been considered a potential candidate for targeted therapy of this breast cancer subtype.

TNBC, however, is a heterogeneous disease in terms of clinical, histological, and molecular aspects[13]. Tumor heterogeneity contributes greatly to the variability in breast cancer treatment response. Therefore, it is important to define reliable markers that can predict the outcome of treatment with targeted drugs. Previous studies have demonstrated variable responses to everolimus in TNBC, and robust molecular biomarkers for prediction of response/resistance to treatment are not yet identified[14]. Metabolites are more representative of the phenotype than genes and proteins, being both downstream products and upstream effectors of gene and protein

signaling, and altered metabolism is one of the more recently acknowledged hallmarks of cancer[15]. Consequently, it has been suggested that metabolic biomarkers or global metabolic profiles can guide patient selection for targeted drug treatment, and detect response/resistance to therapy[16]. High resolution (HR) magic angle spinning (MAS) magnetic resonance spectroscopy (MRS) allows for non-destructive, ex-vivo analysis of biological tissue samples and has been applied to study cancer-related metabolic pathways[17-18]. Cao et al.[19] applied this technique to metabolically characterize TNBC and demonstrated that it was metabolically different from ER+/PgR+/HER2+ breast cancer. In addition, tumors from the same gene expression subtype have been shown to have a variety of different metabolic profiles, as assessed by HR MAS MRS[20-21]. The potential of HR MAS MRS in assessing response to therapy on a metabolic level has also been studied, with metabolic profiles discriminating responders from non-responders and relating metabolic changes after treatment in 5-year survival[22-24] . Moestue et al. have demonstrated how response to treatment with a dual PI3K/mTOR inhibitor, BEZ235, was associated with altered levels of choline-containing metabolites as well as altered glucose and lactate levels in basal-like breast cancer xenografts[7].

The objective of this study was to assess whether metabolic profiles can predict response to treatment with everolimus in a heterogeneous panel of TNBC patient-derived xenografts (PDX). Using HR MAS MRS, we aimed to identify metabolic biomarkers for response/resistance. We additionally explored whether the expression, phosphorylation, or mutation status of molecules regulating PI3K/AKT signaling could be determined based on metabolite information.

MATERIALS AND METHODS

Ethics

All procedures and experiments involving animals were carried out according to the institutional guidelines of the French Ethical Committee and the European Convention for the Protection of Vertebrates used for Scientific Purposes.

Animal Models

Thirteen TNBC PDX were previously established as described in [25]; the models have been further subclassified based on gene expression profiles (Table 1). Treated animals (n = 4 per PDX model, $n_{treated}$=50) received everolimus (Novartis, Basel, Switzerland) at an oral dose of 2.5 mg/kg three times a week for 4-5 weeks; fifty three animals (n = 4 per PDX model) were untreated controls, resulting in tumor tissue samples from a total of 103 animals (Figure 2)*. The tumor tissue was harvested on the last day of treatment, snap-frozen immediately, and stored at -80°C. TNBC xenograft molecular and histological traits, previously characterized, are summarized in Table 1; for further information on the effect of everolimus treatment on protein and gene expression for this cohort, refer to [14].

* Although the study was designed to include eight animals, i.e. n=4 treated animals and n=4 untreated controls, per PDX model, this number varied due to e.g. limited tumor tissue availability or exclusion of spectra of poor technical quality.

Table 1. Patient-derived tumor xenograft characteristics.

PDX model	nTreated/ nControls	TNBC subtype	PTEN expression	pAKT expression	p53 mutations	Response Group
HBCx2	4/4	Luminal-like (AR+FOXA+)	+	+	p.A276D	Non-Resp.
HBCx12A	2/4	HER2 enriched	-	+	WT	Non-Resp.
HBCx16	4/4	Basal (KRT5+KRT17+)	+	+	WT	Non-Resp.
HBCx30	4/4	Basal (KRT5+KRT17+)	-	-	p.F134L	Non-Resp.
HBCx39	4/4	Basal (KRT5+KRT17+) / HER2 enriched	+	-	p.Y220C	Responder
HBCx31	4/4	Luminal-like (AR+FOXA1+)	+	+	p.R175H	Responder
HBCx66	4/4	Basal (KRT17+)	-	+	p.R273C	Responder
HBCx10	4/4	HER2 enriched	-	+	p.Q144fs	Responder
HBCx51	3/2	HER2 enriched	+	-	p.R337C	Responder
HBCx4B	7/8	Basal (KRT5+ KRT17+)	-	+	p.S149fs	Responder
HBCx52	3/4	Luminal-like AR+ FOXA1+	+	NA	p.E336X	Responder
HBCx24	4/3	Basal (KRT5+)	-	+	p.K292fs	Responder
HBCx63	3/4	unclassified	-	+	p.R175H	Responder

All PDX models were of the invasive ductal carcinoma (IDC) histological type.

AR: androgen receptor; FOXA: forkhead box protein A; KRT: keratin; NA: not available; Non-resp.: non-responder; PDX: patient-derived xenograft; TNBC: triple negative breast cancer; WT:wild type.

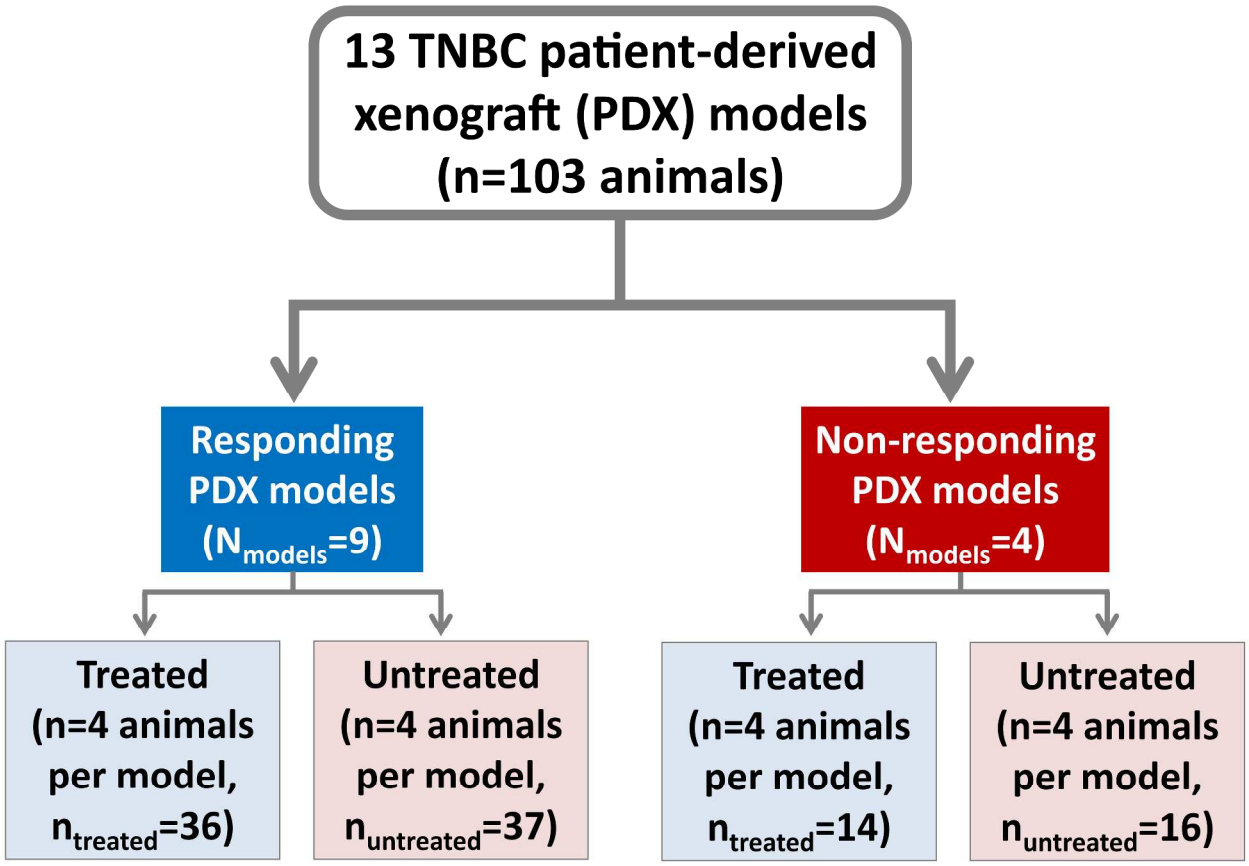

Figure 2. Study Design. Thirteen triple negative breast cancer (TNBC) patient-derived xenograft (PDX) models were included in the study. Nine PDX models were found to respond to everolimus based on significant differences in relative tumor volume between treated animals and untreated controls. For each PDX model, approximately 4 animals were treated with everolimus and 4 were untreated controls. The total number of samples obtained were $n_{treated}$=50, and $n_{untreated}$=53.

Evaluation of Treatment Response

Response was classified based on relative tumor volume (RTV) measured using external calipers. For each PDX model, a Student's t test was performed comparing the RTV of treated tumors with that of the untreated tumors at the end of the treatment period. PDX models

exhibiting a significant difference ($p \leq 0.05$) in RTVs of treated and untreated animals were classified as responders, while those not meeting this criterion were classified as non-responders.

HR MAS MRS analysis

Tumor tissue samples (12.29 ± 2.97 mg) were prepared and analyzed as described in the HR MAS MRS protocol by Giskeødegård et al.[26]. In short, samples were cut on a dedicated, cooled work station to fit into 30 µL disposable inserts containing 3.0 µL of 24.29 mM sodium formate (VWR BDH Prolabo, France) in D2O (Armar Chemicals, Switzerland) for shimming and locking purposes. Each insert was set tightly into a 4 mm MAS zirconium rotor. Each sample was prepared within five minutes, and HR MAS MR spectra were subsequently acquired on a Bruker Avance DRX600 spectrometer (Bruker Biospin GmbH, Germany) equipped with a 1H/13C MAS probe. Samples were spun at 5 kHz while maintaining the probe temperature at 5°C to minimize tissue degradation. Proton spectra were acquired using a spin-echo Carr-Purcell Meiboom-Gill (CPMG) sequence (cpmgpr1d, Bruker BioSpin, Germany) as previously described in [21], with effective echo time of 77 ms, a spectral width of 20 ppm (−5 to 15 ppm), and 256 scans.

Immunohistochemical staining and mutation screening

Formalin-fixed, paraffin-embedded samples were analyzed by immunohistochemistry for the expression of phosphatase and tensin homolog (PTEN) and pAKT as described in [14]. Mutations in the tumor suppressor gene p53 were screened for as described in Supplementary Methods (Supporting Information).

Data preprocessing

From the original sample cohort of 108 samples, four were excluded due to high levels of an unknown contaminant at 3.70 ppm and one for poor spectral quality, resulting in 103 samples for subsequent statistical analysis. Following acquisition, the free induction decays (FIDs) were Fourier transformed into 64k real points after 0.30 Hz line broadening. Phase correction was performed automatically for each spectrum using TopSpin 3.1 (Bruker BioSpin GmbH, Germany).

The following spectral preprocessing steps were performed in Matlab R2013b (The Mathworks, Inc., USA). The spectral region between 1.40 – 4.70 ppm, containing the majority of low-molecular weight metabolites, was selected for further processing. Chemical shifts were referenced to the creatine peak at 3.03 ppm. The spectra were baseline corrected using asymmetric least squares[27] with parameters λ = 1e7 and p = 0.0001, after setting the lowest point in each spectrum to zero. Peak alignment was carried out using icoshift[28]. Lipid peaks at 4.33–4.28, 4.18–4.13, 2.88–2.72, 2.30–2.21, 2.11–2.00, 1.65–1.55 ppm, and the contaminant peaks for the previously mentioned unknown compound and ethanol at 3.73–3.69 and 3.67–3.62 ppm, respectively, were excluded from further analysis. The resulting spectra were normalized to total area to correct for differences in sample size and tumor cell content.

Statistical Analysis

Metabolite peak assignment was performed based on previous identification[29]. Seventeen metabolites were identified as measurable. Their relative levels were calculated by integrating fixed regions of preprocessed spectra corresponding to the metabolite of interest in Matlab R2013b. The metabolite ratios of lactate/glucose, taurine/creatine, and glycerophosphocholine/phosphocholine were determined, and were combined with the relative levels of individual metabolites to make a single dataset which will be referred to as *metabolite*

integrals. All metabolite integrals were log10 transformed (Table S-1, Supporting Information) to satisfy prerequisite assumptions of normality of analyses of individual metabolites.

Multivariate analysis

Multivariate analysis was carried out for metabolite integrals in Matlab R2013b (The Mathworks, Inc., USA) using PLS Toolbox 7.8.2 (Eigenvector Research Inc., U.S.A). The log10 transformed integrals were autoscaled prior to multivariate model building. Principal component analysis (PCA)[30] was performed on metabolite data from the whole dataset, as well as from untreated controls and treated xenografts separately, to explore naturally-occurring trends for different PDX models. The optimal number of principle components (PCs) was selected based on visual inspection of residual explained variance plots. Partial least squares-discriminant analysis (PLS-DA)[31] was used to build a classification model of all samples to discriminate treated xenografts from untreated controls. Additional classification models were also built for treated xenografts and untreated controls separately, to discriminate between responding and non-responding PDX models. Finally, PLS-DA was employed to build models of untreated controls discriminating tumors expressing (+) or not expressing (–) PTEN and pAKT, as well as tumors with mutant or wild type p53. PCA and PLS-DA loadings plots were employed to relate variables or metabolites to samples or xenografts in the scores plots. For PLS-DA plots, orthogonal PLS (OPLS)[32] was employed to condense the y-variance into the first latent variable (LV) when the number of optimal LVs >1.

The PLS-DA classification performance parameters of accuracy, sensitivity, and specificity were obtained by employing double-layered cross validation (CV)[33] to avoid model overfitting. This method optimizes the number of PLS LVs in the inner CV layer and assesses model predictive ability in the outer layer. The procedure consisted of splitting the samples into a training and test

set in each layer; this was performed by randomly selecting 20% of the samples to be excluded from model building, or training, for subsequent testing of the model built. The splitting was repeated until each sample was used for testing once and only once, keeping all animals of the same PDX model type together in either the training or test set. A maximum of ten LVs were considered for optimization. The whole double CV procedure was repeated 20 times, with the final classification results and optimal number of LVs resulting from the mean and mode, respectively. For PLS-DA discrimination of p53 mutation status, double-layered CV was not possible because only two PDX model types had wild type p53 (Table 1). Therefore, for this PLS-DA model only, leave-one-PDX type-out CV was performed instead. Permutation testing[33] was carried out as an additional model validation. For this, the sample class labels were randomly shuffled (permuted) before PLS-DA model building. Permuted models were assessed in the same manner as their non-permuted counterparts using the previously determined optimal number of LVs from double-layered CV or leave-one-PDX type-out CV. A thousand permutations were performed for each non-permuted model being validated, obtaining a permuted accuracy distribution. Models were considered significant if the final accuracy obtained from non-permuted double CV was higher than 95% of the permuted accuracy values ($p \leq 0.05$).

Analysis of individual metabolites

To compare treated xenografts versus untreated controls and responding versus non-responding PDX models simultaneously, linear mixed-effects models (LMM)[34] were employed as a multilevel approach. LMMs incorporate two types of effects to describe relationships between a response variable and different categorical factors. Fixed effects are controlled and systematic, originating from differences between factor levels, while random effects originate from the

between-PDX model variation, each being derived from a different patient. Here, a LMM was built in R 3.1.1[35] using the function lme from the *nlme* package[36] and the method of restricted maximum likelihood. The response variable was the metabolite level, the fixed effects were treatment group (treated or untreated) and response group (responding or non-responding PDX), and the random effect was the PDX model.

LMM was additionally employed to correct for repeated PDX model measurements while determining individual metabolite differences between treated xenografts and untreated controls in responding and non-responding PDX models separately. These two LMM were built as described above, except that only the treatment group fixed effect was included, as samples were divided to perform the analysis on each individual response group. All LMM were built without interaction terms after determining that interactions were not significant, as described in[24]. Obvious deviations from normality were not observed from LMM residual q-q plots and histograms.

LMM p-values were corrected for multiple testing by the Benjamini Hochberg method for false discovery rate (FDR) adjustment in R 3.1.1 using the *stats* package[35]. Adjusted p (q-value) $\leq$ 0.05 was considered to be statistically significant.

RESULTS AND DISCUSSION

Triple negative breast cancer is the most clinically challenging histopathological category of the disease owing to its highly aggressive nature, poor prognosis, and lack of available targeted therapies[37]. Activation of the PI3K signaling pathway is frequently seen in TNBC, and it has therefore been proposed that drugs targeting the PI3K/AKT/mTOR axis may be of particular benefit in these patients. It has been suggested that metabolic biomarkers may be used to predict

or monitor response to targeted drugs in breast cancer. In this study, we used MR spectroscopy to obtain metabolic profiles from patient-derived triple negative breast tumor xenografts following everolimus treatment and untreated controls, demonstrating more pronounced metabolic effects in responding xenografts compared to non-responders. Since this drug blocks PI3K signaling via mTOR inhibition, we additionally explored whether metabolic data reflects the expression of key proteins and mutation status for the tumor suppressor gene p53, which regulate signaling activity in this pathway.

Metabolic effects of everolimus treatment

PLS-DA of 20 metabolite integrals from all samples was performed to discriminate between treated xenografts and untreated controls (Figure 3A), achieving an accuracy of 67% ($p=0.003$) (Table 2). Treated xenografts exhibited higher glucose, glutamine, and alanine levels, and lower phosphocholine (PCh), glycerophosphocholine (GPC), and lactate/glucose (Lac/Glc) (Figure 3B). However, no clear separation between treatment groups could be observed with PCA (Figure S-1, Supporting Information). Nevertheless, when employing LMM as a multilevel approach, the same metabolites deemed important through PLS-DA, with the exception of GPC/PCh instead of GPC, were found to be significantly different for the fixed effect of treatment group after multiple testing correction (Table 3), with coefficients agreeing with PLS-DA loading trends; this indicates that both PLS-DA and LMM revealed the same metabolic alterations in TNBC patient-derived tumor xenografts, summarized by pathway in Figure 4, following everolimus treatment. Mean metabolite values for treated xenografts and untreated controls are presented in Table S-2 (Supporting Information).

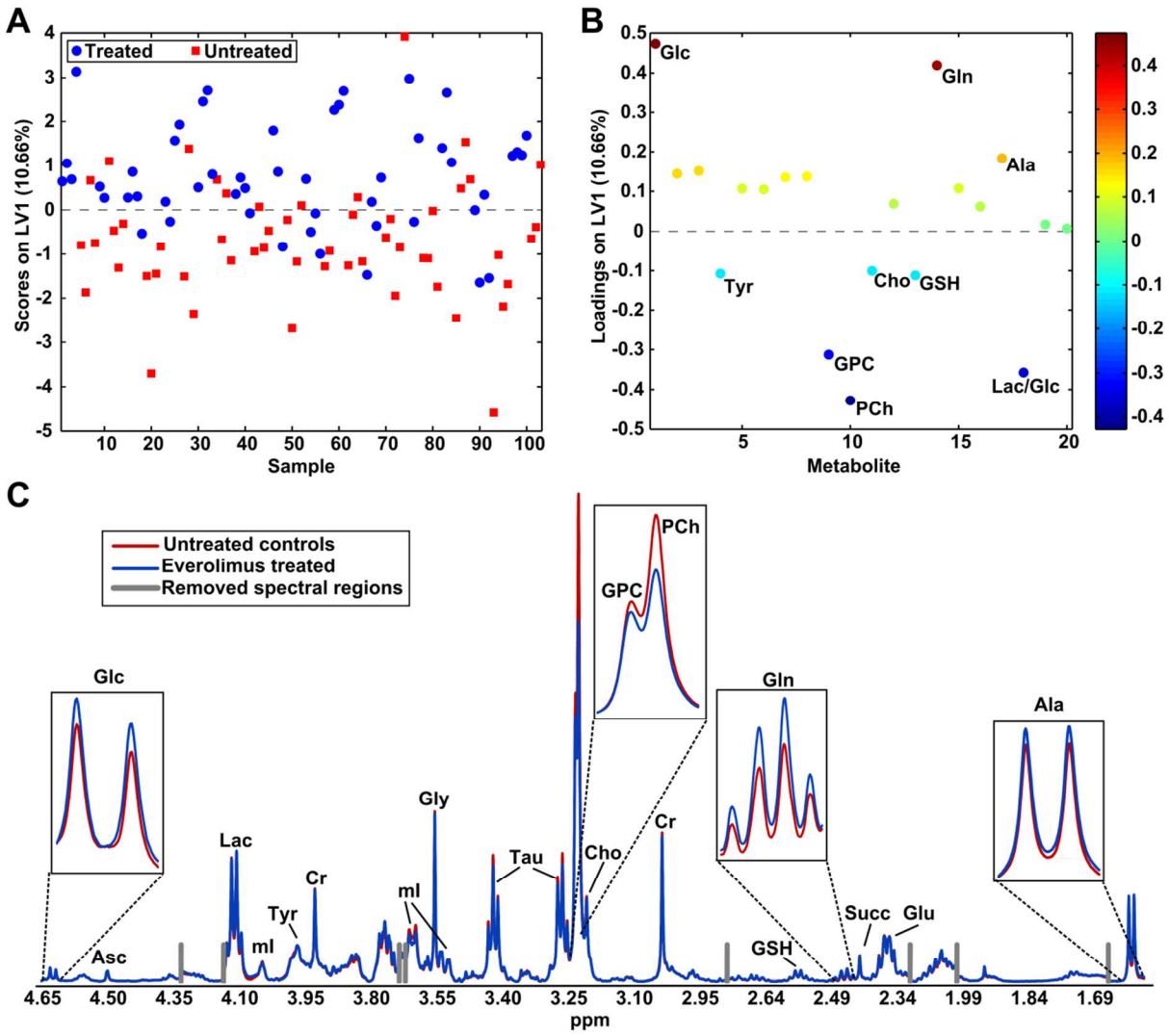

Figure 3. PLS-DA scores (A) and loadings plots (B) of treated xenografts vs untreated controls (n=103), and mean spectra (C) of treated xenografts and untreated controls. Treated xenografts exhibit higher score values on latent variable (LV) 1 compared to untreated controls (A). Metabolites exhibiting higher loading values (B) are higher in treated xenografts compared to controls. Loadings are colored according to LV 1. Ala: alanine; Asc: ascorbate; Cho: choline; Cr: creatine; Glc: glucose; Gln: glutamine; Glu: glutamate; Gly: glycine; GPC: glycerophosphocholine; GSH: glutathione; Lac: lactate; mI: myo-inositol; PCh: phosphocholine; Succ: succinate; Tau: taurine; Tyr: tyrosine.

Table 2. Classification results from PLS-DA.

Samples included in the model	Discriminated Classes	n	No. of LVs	Classification Accuracy (%)	Sensitivity/ Specificity (%)	Permutation p-value
All	Treated vs Untreated	103	1	67	66/68	0.003*
Untreated	Resp. PDX vs Non-resp. PDX	53	1	47	63/32	0.613
Treated	Resp. PDX vs Non-resp. PDX	50	1	57	68/46	0.237
Untreated	PTEN+ vs PTEN-	53	1	63	68/57	0.069
Untreated	pAKT+ vs pAKT-	49[#]	1	57	21/94	0.244
Untreated	p53 mutant vs Wild type	53	1	87	74/100	0.001*

Sensitivity/Specificity are reported for Treated/Resp. PDX /PTEN+/pAKT+/p53 mutant.
* indicates significant p-values (≤0.05).
[#]4/53 samples were of a PDX model with undetermined pAKT expression, and were therefore excluded.
n: number of samples; No. of LVs: number of latent variables; Resp. PDX: Responding patient-derived xenograft models; Non-resp PDX: non-responding patient-derived xenograft models; Class: classification.

Table 3. LMM results for the fixed effects of treatment group and response group.

Metabolite	Treated xenografts vs untreated controls			Responding vs non-responding PDX		
	Coefficient	Std. Error	q-value	Coefficient	Std. Error	q-value
Glc	0.130	0.038	4.45E-03*	-0.049	0.116	9.25E-01
Asc	0.016	0.019	6.63E-01	0.186	0.063	2.51E-01
Lac	0.015	0.018	6.63E-01	-0.057	0.055	8.39E-01
Tyr	-0.012	0.021	8.82E-01	0.045	0.065	9.09E-01
Gly	0.015	0.017	6.63E-01	0.008	0.077	9.76E-01
mI	0.007	0.018	9.24E-01	-0.054	0.126	9.25E-01
Tau	-0.004	0.021	9.24E-01	0.002	0.055	9.76E-01
sI	0.038	0.040	6.63E-01	0.028	0.118	9.59E-01
GPC	-0.035	0.025	4.80E-01	0.093	0.165	9.25E-01
PCh	-0.129	0.028	1.26E-04**	0.032	0.093	9.25E-01
Cho	-0.006	0.022	9.24E-01	0.054	0.051	8.39E-01
Cr	-0.003	0.019	9.28E-01	0.103	0.112	8.39E-01
GSH	0.007	0.027	9.24E-01	-0.054	0.057	8.39E-01
Gln	0.144	0.021	2.59E-08**	0.115	0.098	8.39E-01
Succ	0.019	0.018	6.63E-01	0.040	0.041	8.39E-01
Glu	0.007	0.019	9.24E-01	-0.081	0.061	8.39E-01
Ala	0.060	0.015	7.02E-04**	-0.071	0.075	8.39E-01
Lac/Glc	-0.115	0.041	2.05E-02*	-0.008	0.132	9.76E-01
Tau/Cr	0.000	0.015	9.87E-01	-0.103	0.128	8.83E-01
GPC/PCh	0.095	0.025	1.63E-03*	0.059	0.172	9.25E-01

The coefficients reflect the difference in group mean metabolite levels. Metabolite level increase (positive coefficient) or decrease (negative coefficient) is shown for treated xenografts with respect to untreated controls, and for responding PDX models with respect to non-responding PDX models. * and ** indicate significance ($q \leq 0.05$ and $q \leq 0.001$, respectively).

Ala: alanine; Asc: ascorbate; Cho: choline; Cr: creatine; Glc: glucose; Gln: glutamine; Gly: glycine; Glu: glutamate; GPC: glycerophosphocholine; GSH: glutathione; Lac: lactate; mI:

myo-inositol; PCh: phosphoscholine; sI: scyllo-inositol; Std.: standard; Succ: succinate; Tau: taurine; Tyr: tyrosine.

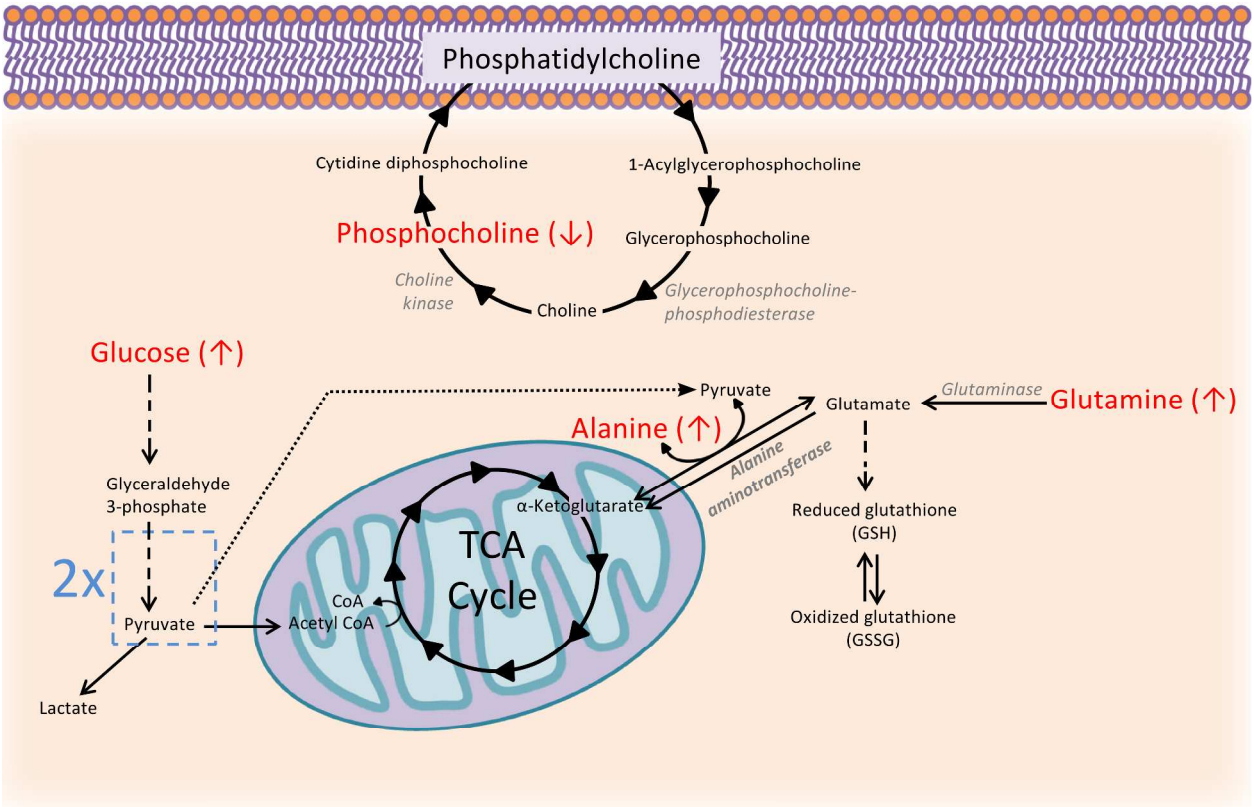

Figure 4. Overview of pathways involving metabolites found to be significantly different between treated xenografts and untreated controls. Significantly different metabolites are marked in red, with arrows indicating the trend in treated xenografts with respect to untreated controls. Related enzymes are marked in gray.

PI3K activation has been shown to drive glucose consumption and, subsequently, lactate production[38]. This is often reflected in low levels of glucose and high levels of lactate in tumor tissue[39-41], and was found by Moestue et al. in basal-like xenografts following PI3K inhibition[7]. The expected reduced lactate-to-glucose ratio in everolimus-treated xenografts suggests that inhibition of mTOR led to a decrease in glucose consumption.

The decrease in PCh is also indicative of a positive effect of everolimus treatment. This metabolite is an intermediate in the synthesis of the cell membrane phospholipid phosphatidylcholine (Figure 4), and has been associated with malignant transformation[42]. The relationship between PCh and GPC is currently under discussion, with some studies suggesting increased PCh/GPC as a marker for malignancy[42-43] while others have found the inverse GPC/PCh to be elevated in breast cancer subtypes with worse prognosis[44-45]. Here, GPC/PCh was observed to be significantly higher in the treated xenografts compared to untreated controls, while no significant differences were observed for either GPC or choline. This suggests that PCh is the total choline (tCho)-constituent most affected by everolimus, and its decrease may reflect a reduction in tumor malignancy and aggressiveness due to everolimus treatment.

Cancer cells depend on glutamine to replace glucose, feeding the TCA cycle via production of alpha-ketoglutarate (Figure 4). In addition, it plays an important role in supplying carbon and nitrogen for macromolecular synthesis needed to sustain cell proliferation[46]. The significantly higher levels of glutamine observed in the treated xenografts suggests its lower consumption in this group, and may reflect a decrease in glutamine addiction with everolimus treatment.

Metabolic differences between responding and non-responding PDX models

The identification of biomarkers for the selection of patients expected to respond to anti-PI3K/AKT/mTOR treatment was one of the current major challenges Hatem et al. aimed to address in [14], where the effect of everolimus treatment on protein and gene expression for the animal cohort included in this study was investigated. Response or resistance could not be successfully associated to the genes and proteins measured at baseline in the said study. Rather, a treatment-induced change, specifically in the phosphorylation of AKT, was suggested as a

potential biomarker for early drug response monitoring. We therefore investigated whether metabolomics could be a feasible approach for prediction of response to everolimus treatment.

Responding and non-responding PDX models could not be discriminated by multivariate PLS-DA, neither using metabolic information from untreated controls nor treated xenografts (Table 2). Similarly, for the multilevel LMM, no metabolites were significantly different for the response group fixed effect. In addition, PCA of untreated controls (Figure 5A) and treated xenografts (Figure 6A) did not reveal any separation between responding and non-responding PDX models. Separate PCA models of untreated controls including only responding (n=37) (Figure 5B) or only non-responding models (n=16) (Figure 5C) were built to explore inherent differences in metabolic profiles between PDX models. These showed clear groupings in the scores plot by PDX model, reflecting the metabolic heterogeneity among the PDX models. This metabolic heterogeneity was expected, as the PDX differed with regards to gene expression traits. Initial inter-tumor metabolic heterogeneity may have therefore contributed to the unsuccessful prediction of response to everolimus treatment. PDX model heterogeneity persisted after everolimus treatment, as evidenced by the groupings in separate PCA models of treated xenografts including only responding (n=36) (Figure 6B) or only non-responding PDX models (n=14) (Figure 6C). Our findings therefore reflect metabolic heterogeneity both independent of (untreated control group) and after everolimus treatment (treated group).

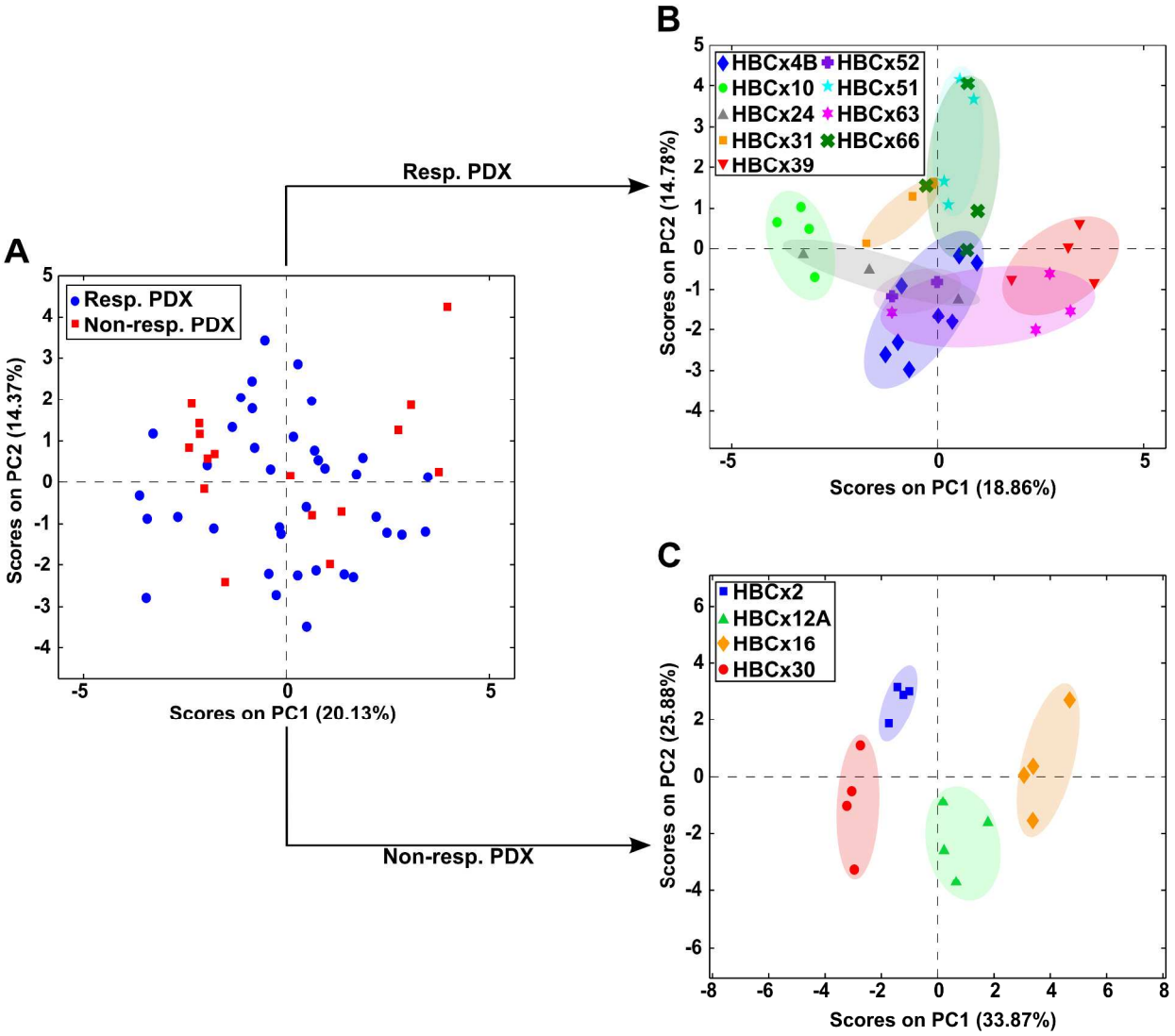

Figure 5. PCA of all untreated controls (A), untreated responding (Resp.) patient-derived xenografts (PDX) only (B), and untreated non-responding (Non-resp.) PDX only (C). Samples in B and C are colored according to PDX model. Xenografts from the same PDX model cluster together (B and C), reflecting a greater variability between PDX models than within PDX models. Ovals were drawn manually to illustrate clusters.

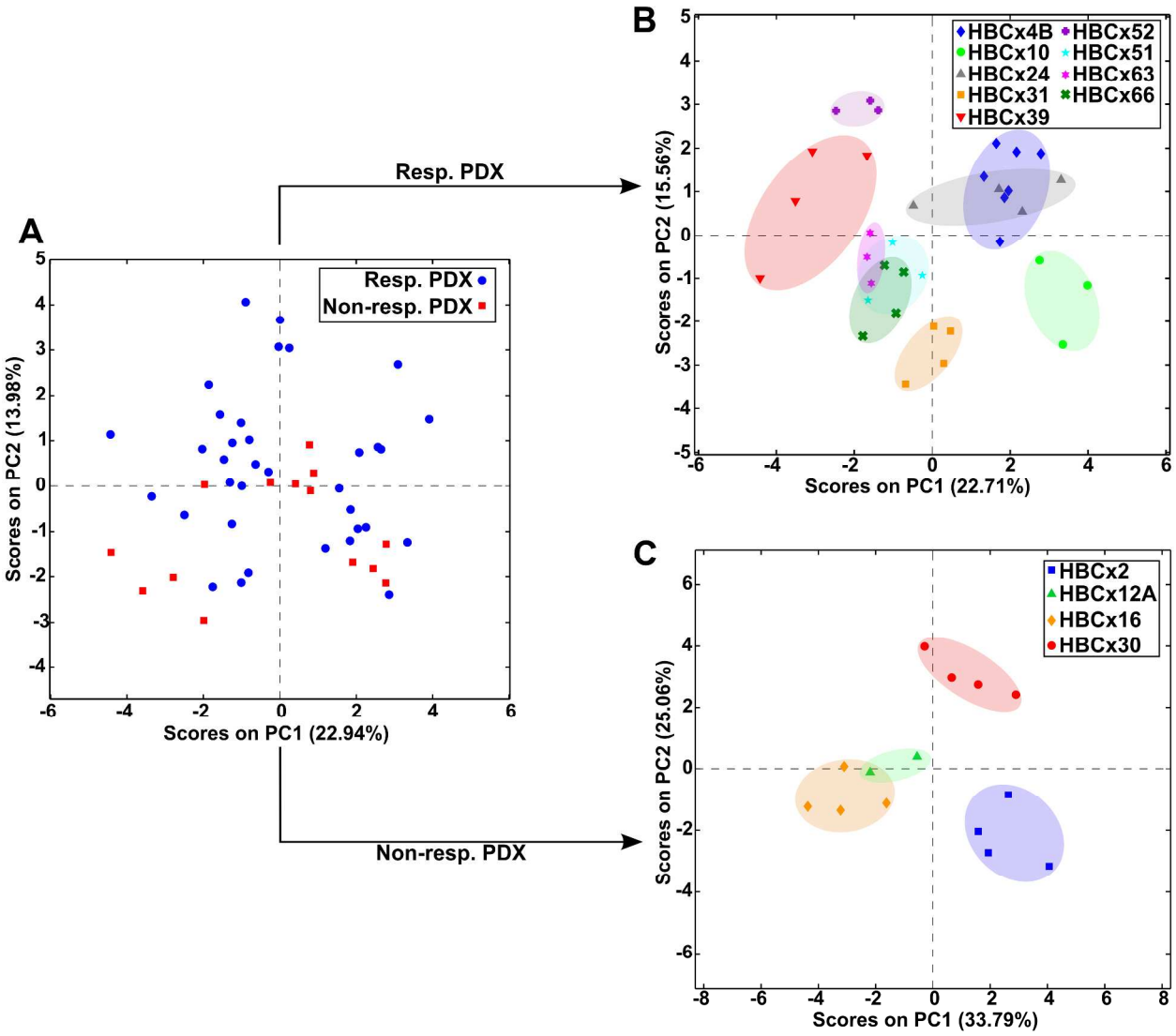

Figure 6. PCA of all treated patient-derived xenografts (PDX) (A), treated responding (Resp.) PDX only (B), and treated non-responding (Non-resp.) PDX only (C). Samples in B and C are colored according to PDX model. Xenografts from the same PDX model cluster together (B and C), reflecting a greater variability between PDX models than within PDX models. Ovals were drawn manually to illustrate clusters.

Building the multilevel LMM including the random effect of PDX model should account for the between-PDX model heterogeneity, but differences between the response groups could still not be detected using this technique. The observed heterogeneity suggests that treatment

management of TNBC may benefit from further stratification of this histopathological subtype. Moestue et al.[7] found that a basal-like, but not a luminal-like, breast cancer PDX responded to PI3K inhibitors, and basal-like cancers have been found to be more homogenous than TNBC[47]. In our cohort, however, both responding and non-responding PDX models included basal-like, luminal-like, and HER2-enriched tumors (Table 1), suggesting that other factors contributed to the heterogeneous treatment efficacy in terms of tumor growth inhibition within the gene expression subtypes. Additional sources of this heterogeneity, perhaps with an initial focus on basal-like breast cancers, may be worth investigating.

When analyzing metabolite information from responding PDX models (n=73) and non-responding PDX models (n=30) separately using LMM to correct for repeated PDX model measurements, individual metabolite differences between treated xenografts and controls were determined within these two groups. For responding models, treated xenografts exhibited significantly higher glucose, glutamine, and alanine, and significantly lower PCh, GPC/PCh, and Lac/Glc compared to untreated controls (Figure 7), which was similar to the findings from LMM of the whole cohort simultaneously (Table 3). For non-responding models, however, only PCh and glutamine were significantly lower and higher, respectively, with treatment (Figure 7). Collectively, these results indicate that the metabolic response to everolimus treatment is more pronounced in responding PDX models, with increased levels of metabolites representing the central carbon metabolism and decreased levels of phosphocholine. Mean metabolite values for each treatment group within responding and non-responding PDX are presented in Table S-3 (Supporting Information).

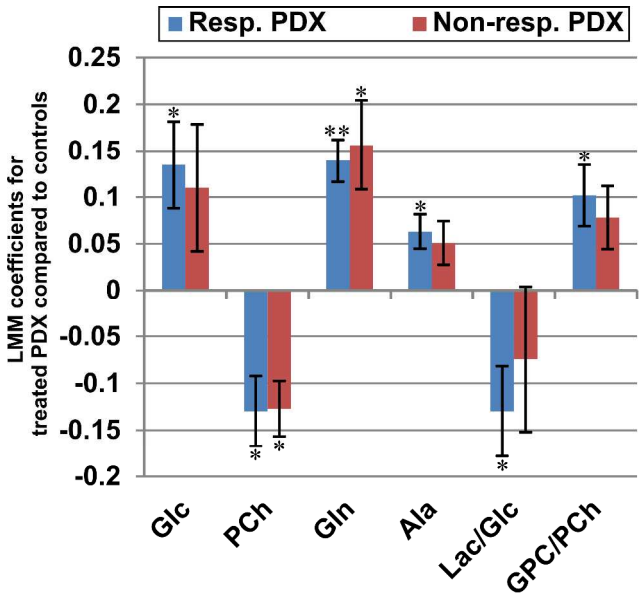

Figure 7. LMM coefficients for treated xenografts compared to untreated controls carried out separately for responding models (Resp. PDX) and non-responding models (Non-resp. PDX). * and ** indicate significance ($q \leq 0.05$ and $q \leq 0.001$, respectively). Ala: alanine; Glc: glucose; Gln: glutamine; GPC: glycerophosphocholine; Lac: lactate; PCh: phosphocholine.

Significant changes in metabolites involved in glycolysis only in the responding models is consistent with findings from Foster et al.[48], who observed glucose-dependent growth in cells with mutations in PIK3CA, the gene encoding the alpha catalytic subunit of PI3K. In contrast, they found that both wild-type and PIK3CA-mutated cells depended on glutamine to grow. This supports our observed significant increase in glutamine with treatment, independent of whether tumor growth was significantly inhibited (responding PDX) or not (non-responding PDX). Previous work studying the same animal cohort examined here, however, found that PIK3CA mutations were rare and could not predict response to everolimus on their own[14].

Similarly as in Hatem et al.[14], intrinsic metabolic differences (i.e. in the untreated controls) between responding and non-responding PDX could not be identified. Furthermore, we could not

see the differences in AKT activation they observed being translated to the metabolic level, as the metabolite information could not discriminate post treatment samples expressing or not expressing pAKT (results not shown). Findings related to response were not as easily identified as metabolic differences between treated and untreated xenografts. This reflects the findings of Hatem et al., demonstrating how breast cancer heterogeneity makes it difficult to identify generic biomarkers for response and resistance.

It is important to note that the response criteria used here was based on tumor size, since this is the traditional approach. Imaging techniques are widely used in the clinic to assess response to treatment based on tumor size reduction[49-50]. There has been increasing interest in the development of imaging modalities that can detect biological and physiological changes in tissue rather than just imaging morphology[51-52]. Functional imaging approaches provide possibilities for treatment monitoring based on biological changes in the tumor, which may occur long before any reduction in size[53]. In line with this, we could detect metabolic differences between treated xenografts and untreated controls, pointing to biological changes occurring as an effect of treatment, in all PDX models, whether they exhibited a significant reduction in tumor volume or not. Furthermore, Cao et al.[23] observed a subtle metabolic difference between responders and non-responders classified based on tumor size, while changes in the metabolic profiles following treatment could significantly distinguish long term survivors from non-survivors. Nevertheless, PDX models responding to everolimus therapy in our study exhibited a more significant metabolic response than resistant models.

Metabolic discrimination of PI3K pathway protein expression and p53 mutation status

Since the metabolic profile is affected by the genetic and proteomic make-up, we investigated the association between metabolite information and key molecules regulating PI3K/AKT

signaling measured by Hatem et al.[14] in an effort to gain insight on PI3K signaling mechanisms. Protein expression determined from immunohistochemistry and p53 mutation status for the PDX models is given in Table 1. PLS-DA results to classify untreated controls (n=53) according to expression or no expression of proteins PTEN and pAKT and to p53 mutation status are summarized in Table 2. Metabolite integrals were unable to predict pAKT expression, while PTEN expression discrimination approached significance (Accuracy=63%, p=0.069) (Figure 8C).

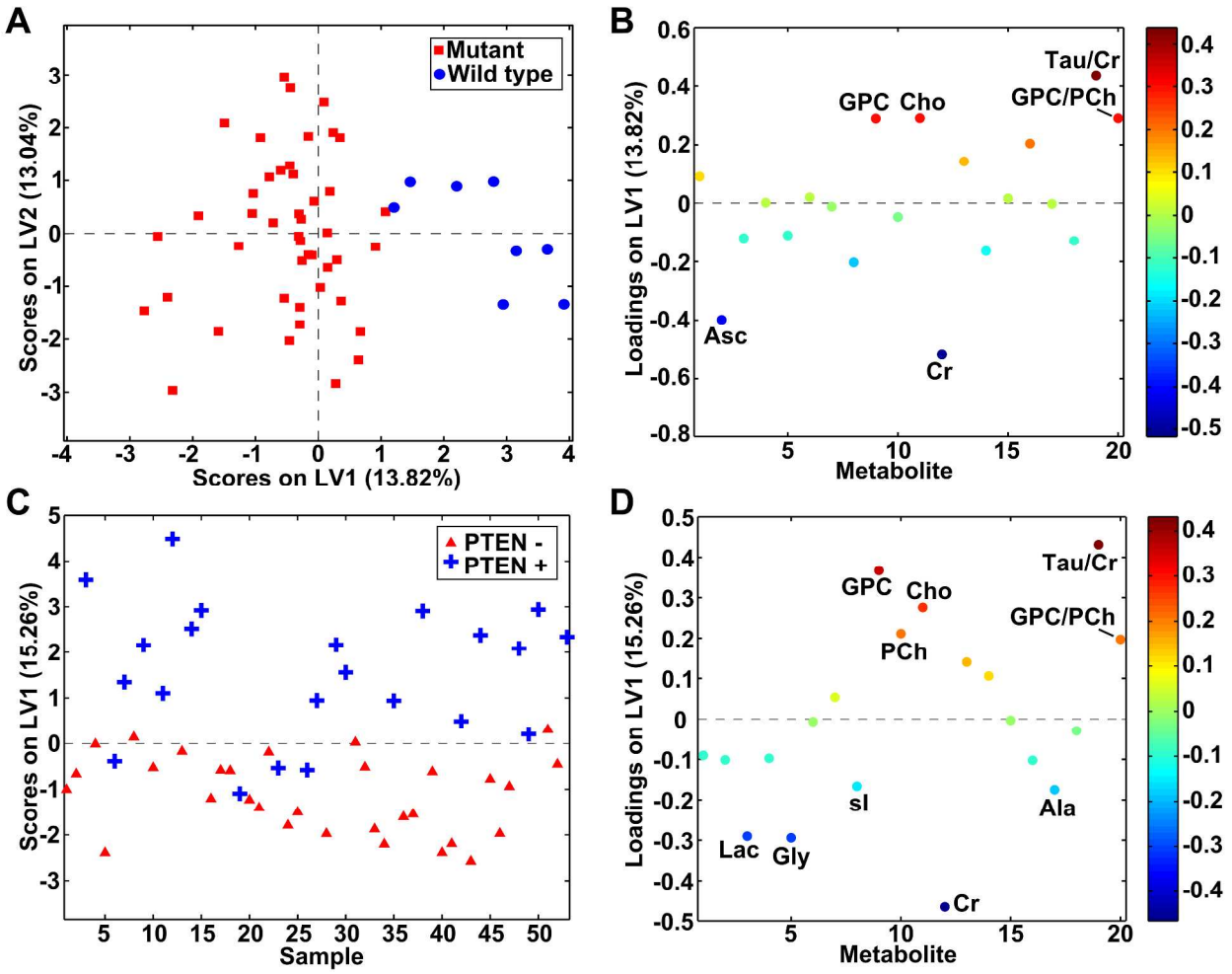

Figure 8. PLS-DA scores (A) and loadings plots (B) of p53 mutant vs p53 wild type untreated controls, and PLS-DA scores (C) and loadings plots (D) of PTEN- vs PTEN+ untreated controls. Wild type p53 and PTEN + xenografts exhibit higher score values on latent variable (LV) 1 compared to mutant p53 (A) and PTEN – (C), respectively. Loadings plots (B and D) show similar metabolic trends differentiating p53 mutation status and PTEN expression, with metabolites exhibiting higher loading values being higher in Wild type p53 and PTEN + xenografts compared to mutant p53 and PTEN –, respectively. Loadings are colored according to LV 1. Ala: alanine; Asc: ascorbate; Cho:Choline; Cr: creatine; Gly: glycine; GPC: glycerophosphocholine; Lac: lactate; PCh: phosphocholine; sI: scyllo-inositol; Tau: taurine.

p53 mutation status was successfully discriminated with an accuracy of 87% (p=0.001) (Figure 8A), with the mutant gene associated with increased ascorbate and creatine, and decreased GPC and choline (Figure 8B). It should be noted, however, that double-layered cross validation could not be performed for the discrimination of p53 mutation status because only two PDX model types were p53 wild type. Leave-one-PDX type-out CV was therefore performed instead, which tends to produce a much more optimistic accuracy than double-layered CV. Still, wild type p53 exhibited similar metabolic trends for creatine, GPC, and choline as PTEN expression (Figure 8B, Figure 8D). Since PTEN is another tumor suppressor, this indicates that the expression of tumor suppressor genes regulating signal transduction in the PI3K pathway is reflected in the metabolic profile of the tumor.

The potent tumor suppressor p53 is involved in cell cycle control via transcriptional regulation of its target genes. p53 increases guanidinoacetate methyltranferase (GAMT), which catalyzes the production of creatine from guanidinoacetate (GAA)[54]. Our observed differences in creatine levels between wild type and mutant p53 PDX models may therefore reflect a p53-associated

dysregulation of creatine synthesis. This may result as a compensation mechanism for impaired glycolytic energy production in mutants, since creatine metabolism is tightly connected with ATP homeostasis via the reversible phosphorylation of creatine by creatine kinase with ATP/ADP[55].

CONCLUSION

Clear metabolic differences between everolimus-treated xenografts and untreated controls were detected, indicating reduced glycolytic lactate production and glutaminolysis after treatment, consistent with PI3K/AKT signaling pathway inhibition. Although inherent metabolic heterogeneity between different PDX models seemed to hinder prediction of treatment response, significant changes in glucose, alanine, lactate/glucose, and glycerophosphocholine/phosphocholine with treatment were detected in responding, but not in non-responding, PDX models. p53 mutation status could be predicted using MR based metabolite levels, which may provide complimentary insight into the interplay between PI3K signaling and other drivers of disease progression.

Supporting Information. The following files are available free of charge:

SupportingInformation.pdf. Supporting information including supplementary methods, supplementary figures, and supplementary tables.

SupplementaryTable1.xlsx. Supplementary Table 1 containing metabolite relative levels per PDX model.

Corresponding Author

*Leslie R. Euceda, Department of Circulation and Medical Imaging - MR Center, Faculty of Medicine and Health Sciences, NTNU, Norwegian University of Science and Technology,

Postboks 8905, Medisinsk Teknisk Forskningssenter, 7489 Trondheim, Norway; Phone: +47 73597449, Fax: +47 73598613, E.mail: leslie.e.wood@ntnu.no.

Author Contributions

LRE, DKH, IB, EM, TFB, and SAM participated in the design of the study. IB, EM, and SAM conceived the study. LRE, DKH, EM, TFB, and SAM interpreted the data. ES performed the HR MAS MRS acquisition. LRE performed statistical analysis and drafted the manuscript. RH, REB, IB, EM, TFB, and SAM participated in acquisition of the data. All authors have given approval to the final version of the manuscript.

Funding Sources

This study was funded in part by The Research Council of Norway: Imaging the breast cancer metabolome (Project no. 221879), The Norwegian Cancer Society (Grant no. 2209215), and The Institut Curie (Grant no. 2013-004).

Acknowledgements

The HR MAS MRS analysis was performed at the MR Core Facility, Norwegian University of Science and Technology (NTNU), which is funded by the Faculty of Medicine and Health Sciences at NTNU and Central Norway Regional Health Authority. High-throughput sequencing has been performed by the ICGex NGS platform of the Institut Curie supported by the grants ANR-10-EQPX-03 (Equipex) and ANR-10-INBS-09-08 (France Génomique Consortium) from the Agence Nationale de la Recherche (“Investissements d’Avenir” program), by the Canceropole Ile-de-France and by the SiRIC-Curie program - SiRIC Grant “INCa-DGOS-4654”. We thank Sylvain Baulande who performed the NGS and Virginie Bernard who performed the bioinformatics analysis.

Abbreviations

CPMG, Carr-Purcell Meiboom-Gill; CV, cross validation; ER, estrogen receptor; FDR, false discovery rate; FID, free induction decay; GAA, guanidinoacetate; GAMT, guanidinoacetate methyltransferase; GPC, glycerophosphocholine; GSH, glutathione; HER2, human epidermal growth factor receptor 2; HR MAS MRS, high resolution magic angle spinning magnetic resonance spectroscopy; IDC, invasive ductal carcinoma; Lac/Glc, lactate-to-glucose ratio; LMM, linear mixed-effects model; LV, latent variable; mTOR, mammalian target of rapamycin; PCA, principal component analysis; PCh, phosphocholine; PDX, patient-derived xenograft; PFS, progression-free survival; PgR, progesterone receptor; PI3K, phosphatidylinositol-3-kinase; PLS-DA, partial least squares-discriminant analysis; PTEN, phosphatase and tensin homolog; RTV, relative tumor volume; tCho, total choline; TNBC, triple negative breast cancer.

REFERENCES

1. Giordano, S. H.; Buzdar, A. U.; Smith, T. L.; Kau, S.-W.; Yang, Y.; Hortobagyi, G. N., Is breast cancer survival improving? *Cancer* **2004,** *100* (1), 44-52.
2. American Cancer Society, *Global Cancer Facts & Figures 2nd Edition*. American Cancer Society: Atlanta, GA, USA, 2011.
3. Yiannakopoulou, E., Breast Cancer Therapy–Classical Therapy, Drug Targets, and Targeted Therapy. In *Omics Approaches in Breast Cancer*, Barh, D., Ed. Springer India: 2014; pp 483-498.
4. Perou, C. M.; Sorlie, T.; Eisen, M. B.; van de Rijn, M.; Jeffrey, S. S.; Rees, C. A.; Pollack, J. R.; Ross, D. T.; Johnsen, H.; Akslen, L. A.; Fluge, O.; Pergamenschikov, A.; Williams, C.; Zhu, S. X.; Lonning, P. E.; Borresen-Dale, A.-L.; Brown, P. O.; Botstein, D., Molecular portraits of human breast tumours. *Nature* **2000,** *406* (6797), 747-752.
5. Sørlie, T.; Tibshirani, R.; Parker, J.; Hastie, T.; Marron, J. S.; Nobel, A.; Deng, S.; Johnsen, H.; Pesich, R.; Geisler, S.; Demeter, J.; Perou, C. M.; Lønning, P. E.; Brown, P. O.; Børresen-Dale, A.-L.; Botstein, D., Repeated observation of breast tumor subtypes in independent gene expression data sets. *Proc. Natl. Acad. Sci. U. S. A.* **2003,** *100* (14), 8418-8423.
6. López-Knowles, E.; O'Toole, S. A.; McNeil, C. M.; Millar, E. K. A.; Qiu, M. R.; Crea, P.; Daly, R. J.; Musgrove, E. A.; Sutherland, R. L., PI3K pathway activation in breast cancer is associated with the basal-like phenotype and cancer-specific mortality. *Int. J. Cancer* **2010,** *126* (5), 1121-1131.
7. Moestue, S. A.; Dam, C. G.; Gorad, S. S.; Kristian, A.; Bofin, A.; Mælandsmo, G. M.; Engebråten, O.; Gribbestad, I. S.; Bjørkoy, G., Metabolic biomarkers for response to PI3K inhibition in basal-like breast cancer. *Breast Cancer Res.* **2013,** *15*, R16.

8. Vara, J. Á. F.; Casado, E.; de Castro, J.; Cejas, P.; Belda-Iniesta, C.; González-Barón, M., PI3K/Akt signalling pathway and cancer. *Cancer Treat. Rev.* **2004,** *30* (2), 193-204.
9. Houghton, P. J., Everolimus. *Clin. Cancer Res.* **2010,** *16* (5), 1368-1372.
10. Baselga, J.; Campone, M.; Piccart, M.; Burris, H. A.; Rugo, H. S.; Sahmoud, T.; Noguchi, S.; Gnant, M.; Pritchard, K. I.; Lebrun, F.; Beck, J. T.; Ito, Y.; Yardley, D.; Deleu, I.; Perez, A.; Bachelot, T.; Vittori, L.; Xu, Z.; Mukhopadhyay, P.; Lebwohl, D.; Hortobagyi, G. N., Everolimus in Postmenopausal Hormone-Receptor–Positive Advanced Breast Cancer. *N. Engl. J. Med.* **2012,** *366* (6), 520-529.
11. Ejlertsen, B.; Heinrich, G.; Jerusalem, M.; Hurvitz, S. A.; De Boer, R. H.; Taran, T.; Sahmoud, T.; Burris, H. A., BOLERO-6: Phase II study of everolimus plus exemestane versus everolimus or capecitabine monotherapy in HR+, HER2- advanced breast cancer. *J. Clin. Oncol.* **2013,** *31* (abstr TPS660).
12. André, F.; O'Regan, R.; Ozguroglu, M.; Toi, M.; Xu, B.; Jerusalem, G.; Masuda, N.; Wilks, S.; Arena, F.; Isaacs, C.; Yap, Y.-S.; Papai, Z.; Lang, I.; Armstrong, A.; Lerzo, G.; White, M.; Shen, K.; Litton, J.; Chen, D.; Zhang, Y.; Ali, S.; Taran, T.; Gianni, L., Everolimus for women with trastuzumab-resistant, HER2-positive, advanced breast cancer (BOLERO-3): a randomised, double-blind, placebo-controlled phase 3 trial. *The Lancet Oncology* **2014,** *15* (6), 580-591.
13. Metzger-Filho, O.; Tutt, A.; de Azambuja, E.; Saini, K. S.; Viale, G.; Loi, S.; Bradbury, I.; Bliss, J. M.; Azim, H. A.; Ellis, P.; Di Leo, A.; Baselga, J.; Sotiriou, C.; Piccart-Gebhart, M., Dissecting the Heterogeneity of Triple-Negative Breast Cancer. *J. Clin. Oncol.* **2012**.
14. Hatem, R.; Botty, R. E.; Chateau-Joubert, S.; Servely, J.-L.; Labiod, D.; Plater, L. d.; Assayag, F.; Coussy, F.; Callens, C.; Vacher, S.; Reyal, F.; Cosulich, S.; Diéras, V.; Bièche, I.; Marangoni, E., Targeting mTOR pathway inhibits tumor growth in different molecular subtypes of triple-negative breast cancers. *Oncotarget* **2016**.
15. Hanahan, D.; Weinberg, R. A., Hallmarks of cancer: the next generation. *Cell* **2011,** *144*.
16. Palmnas, M.; Vogel, H., The Future of NMR Metabolomics in Cancer Therapy: Towards Personalizing Treatment and Developing Targeted Drugs? *Metabolites* **2013,** *3* (2), 373.
17. Bathen, T. F.; Sitter, B.; Sjøbakk, T. E.; Tessem, M.-B.; Gribbestad, I. S., Magnetic Resonance Metabolomics of Intact Tissue: A Biotechnological Tool in Cancer Diagnostics and Treatment Evaluation. *Cancer Res.* **2010,** *70* (17), 6692-6696.
18. Moestue, S. A.; Sitter, B.; Bathen, T. F.; Tessem, M.-B.; Gribbestad, I., HR MAS MR Spectroscopy in Metabolic Characterization of Cancer. *Curr. Top. Med. Chem.* **2011,** *11* (1), 2-26.
19. Cao, M. D.; Lamichhane, S.; Lundgren, S.; Bofin, A.; Fjøsne, H.; Giskeødegård, G. F.; Bathen, T. F., Metabolic characterization of triple negative breast cancer. *BMC Cancer* **2014,** *14* (1), 1-12.
20. Borgan, E.; Sitter, B.; Lingjærde, O. C.; Johnsen, H.; Lundgren, S.; Bathen, T. F.; Sørlie, T.; Børresen-Dale, A.-L.; Gribbestad, I. S., Merging transcriptomics and metabolomics - advances in breast cancer profiling. *BMC Cancer* **2010,** *10* (1), 1-14.
21. Haukaas, T. H.; Euceda, L. R.; Giskeødegård, G. F.; Lamichhane, S.; Krohn, M.; Jernström, S.; Aure, M. R.; Lingjærde, O. C.; Schlichting, E.; Garred, Ø.; Due, E. U.; Mills, G. B.; Sahlberg, K. K.; Børresen-Dale, A.-L.; Bathen, T. F., Metabolic clusters of breast cancer in relation to gene- and protein expression subtypes. *Cancer & Metabolism* **2016,** *4* (1), 1-14.

22. Cao, M. D.; Sitter, B.; Bathen, T. F.; Bofin, A.; Lonning, P. E.; Lundgren, S.; Gribbestad, I. S., Predicting long-term survival and treatment response in breast cancer patients receiving neoadjuvant chemotherapy by MR metabolic profiling. *NMR Biomed.* **2012,** *25* (2), 369-78.
23. Cao, M. D.; Giskeødegård, G. F.; Bathen, T. F.; Sitter, B.; Bofin, A.; Lønning, P. E.; Lundgren, S.; Gribbestad, I. S., Prognostic value of metabolic response in breast cancer patients receiving neoadjuvant chemotherapy. *BMC Cancer* **2012,** *12* (1), 1-11.
24. Euceda, L. R.; Haukaas, T. H.; Giskeødegård, G. F.; Vettukattil, R.; Engel, J.; Silwal-Pandit, L.; Lundgren, S.; Borgen, E.; Garred, Ø.; Postma, G.; Buydens, L. M. C.; Børresen-Dale, A.-L.; Engebraaten, O.; Bathen, T. F., Evaluation of metabolomic changes during neoadjuvant chemotherapy combined with bevacizumab in breast cancer using MR spectroscopy. *Metabolomics* **2017,** *13* (4), 37.
25. Marangoni, E.; Vincent-Salomon, A.; Auger, N.; Degeorges, A.; Assayag, F.; de Cremoux, P.; de Plater, L.; Guyader, C.; De Pinieux, G.; Judde, J.-G.; Rebucci, M.; Tran-Perennou, C.; Sastre-Garau, X.; Sigal-Zafrani, B.; Delattre, O.; Diéras, V.; Poupon, M.-F., A New Model of Patient Tumor-Derived Breast Cancer Xenografts for Preclinical Assays. *Clin. Cancer Res.* **2007,** *13* (13), 3989-3998.
26. Giskeodegard, G. F.; Cao, M. D.; Bathen, T. F., High-resolution magic-angle-spinning NMR spectroscopy of intact tissue. In *Metabonomics: Methods and Protocols*, Bjerrum, J. T., Ed. Springer New York: New York, NY, 2015; Vol. 1277, pp 37-50.
27. Eilers, P. H. C., Parametric Time Warping. *Anal. Chem.* **2004,** *76* (2), 404-411.
28. Savorani, F.; Tomasi, G.; Engelsen, S. B., icoshift: A versatile tool for the rapid alignment of 1D NMR spectra. *J. Magn. Reson.* **2010,** *202* (2), 190-202.
29. Sitter, B.; Sonnewald, U.; Spraul, M.; Fjosne, H. E.; Gribbestad, I. S., High-resolution magic angle spinning MRS of breast cancer tissue. *NMR Biomed.* **2002,** *15* (5), 327-37.
30. Wold, S.; Esbensen, K.; Geladi, P., Principal component analysis. *Chemometr Intell Lab* **1987,** *2* (1), 37-52.
31. Wold, S.; Sjöström, M.; Eriksson, L., PLS-regression: a basic tool of chemometrics. *Chemometr Intell Lab* **2001,** *58* (2), 109-130.
32. Eigenvector Research Orthogonalizepls. http://wiki.eigenvector.com/index.php?title=Orthogonalizepls (accessed February 2017).
33. Westerhuis, J.; Hoefsloot, H. J.; Smit, S.; Vis, D.; Smilde, A.; van Velzen, E. J.; van Duijnhoven, J. M.; van Dorsten, F., Assessment of PLSDA cross validation. *Metabolomics* **2008,** *4* (1), 81-89.
34. Pinheiro, J. C.; Bates, D. M., Linear Mixed-Effects Models: Basic Concepts and Examples. In *Mixed-Effects Models in S and S-PLUS*, Springer New York: New York, NY, USA, 2000; pp 3-56.
35. R Core Team (2014) *R: A language and environment for statistical computing*, R Foundation for Statistical Computing: Vienna, Austria. URL http://www.R-project.org/.
36. Pinheiro, J.; Bates, D.; DebRoy, S.; Sarkar, D.; R Core Team (2014), nlme: Linear and Nonlinear Mixed Effects Models. R package version 3.1-117, URL: http://CRAN.R-project.org/package=nlme. **2014**.
37. Kaplan, H. G.; Malmgren, J. A., Impact of Triple Negative Phenotype on Breast Cancer Prognosis. *The Breast Journal* **2008,** *14* (5), 456-463.
38. Plas, D. R.; Thompson, C. B., Akt-dependent transformation: there is more to growth than just surviving. *Oncogene* **0000,** *24* (50), 7435-7442.

39. Gribbestad, I. S.; Petersen, S. B.; Fjosne, H. E.; Kvinnsland, S.; Krane, J., 1H NMR spectroscopic characterization of perchloric acid extracts from breast carcinomas and non-involved breast tissue. *NMR Biomed.* **1994,** *7* (4), 181-94.
40. Tessem, M.-B.; Selnæs, K. M.; Sjursen, W.; Tranø, G.; Giskeødegård, G. F.; Bathen, T. F.; Gribbestad, I. S.; Hofsli, E., Discrimination of Patients with Microsatellite Instability Colon Cancer using 1H HR MAS MR Spectroscopy and Chemometric Analysis. *J. Proteome Res.* **2010,** *9* (7), 3664-3670.
41. Bathen, T. F.; Geurts, B.; Sitter, B.; Fjøsne, H. E.; Lundgren, S.; Buydens, L. M.; Gribbestad, I. S.; Postma, G.; Giskeødegård, G. F., Feasibility of MR Metabolomics for Immediate Analysis of Resection Margins during Breast Cancer Surgery. *PLoS One* **2013,** *8* (4), e61578.
42. Aboagye, E. O.; Bhujwalla, Z. M., Malignant transformation alters membrane choline phospholipid metabolism of human mammary epithelial cells. *Cancer Res.* **1999,** *59* (1), 80-4.
43. Iorio, E.; Ricci, A.; Bagnoli, M.; Pisanu, M. E.; Castellano, G.; Di Vito, M.; Venturini, E.; Glunde, K.; Bhujwalla, Z. M.; Mezzanzanica, D.; Canevari, S.; Podo, F., Activation of phosphatidylcholine-cycle enzymes in human epithelial ovarian cancer cells. *Cancer Res.* **2010,** *70* (5), 2126-2135.
44. Moestue, S.; Borgan, E.; Huuse, E.; Lindholm, E.; Sitter, B.; Borresen-Dale, A. L.; Engebraaten, O.; Maelandsmo, G.; Gribbestad, I., Distinct choline metabolic profiles are associated with differences in gene expression for basal-like and luminal-like breast cancer xenograft models. *BMC Cancer* **2010,** *10*.
45. Giskeodegard, G. F.; Grinde, M. T.; Sitter, B.; Axelson, D. E.; Lundgren, S.; Fjosne, H. E.; Dahl, S.; Gribbestad, I. S.; Bathen, T. F., Multivariate modeling and prediction of breast cancer prognostic factors using MR metabolomics. *J. Proteome Res.* **2010,** *9* (2), 972-9.
46. Hensley, C. T.; Wasti, A. T.; DeBerardinis, R. J., Glutamine and cancer: cell biology, physiology, and clinical opportunities. *J. Clin. Invest.* **2013,** *123* (9), 3678-84.
47. Bertucci, F.; Finetti, P.; Cervera, N.; Esterni, B.; Hermitte, F.; Viens, P.; Birnbaum, D., How basal are triple-negative breast cancers? *Int. J. Cancer* **2008,** *123* (1), 236-240.
48. Foster, R.; Griffin, S.; Grooby, S.; Feltell, R.; Christopherson, C.; Chang, M.; Sninsky, J.; Kwok, S.; Torrance, C., Multiple Metabolic Alterations Exist in Mutant PI3K Cancers, but Only Glucose Is Essential as a Nutrient Source. *PLoS One* **2012,** *7* (9), e45061.
49. Therasse, P.; Arbuck, S. G.; Eisenhauer, E. A.; Wanders, J.; Kaplan, R. S.; Rubinstein, L.; Verweij, J.; Van Glabbeke, M.; van Oosterom, A. T.; Christian, M. C.; Gwyther, S. G., New Guidelines to Evaluate the Response to Treatment in Solid Tumors. *J. Natl. Cancer Inst.* **2000,** *92* (3), 205-216.
50. Eisenhauer, E. A.; Therasse, P.; Bogaerts, J.; Schwartz, L. H.; Sargent, D.; Ford, R.; Dancey, J.; Arbuck, S.; Gwyther, S.; Mooney, M.; Rubinstein, L.; Shankar, L.; Dodd, L.; Kaplan, R.; Lacombe, D.; Verweij, J., New response evaluation criteria in solid tumours: Revised RECIST guideline (version 1.1). *Eur. J. Cancer* **2009,** *45* (2), 228-247.
51. Juweid, M. E.; Cheson, B. D., Positron-Emission Tomography and Assessment of Cancer Therapy. *N. Engl. J. Med.* **2006,** *354* (5), 496-507.
52. Gutte, H.; Hansen, A. E.; Johannesen, H. H.; Clemmensen, A. E.; Ardenkjær-Larsen, J. H.; Nielsen, C. H.; Kjær, A., The use of dynamic nuclear polarization (13)C-pyruvate MRS in cancer. *Am. J. Nucl. Med. Mol. Imaging* **2015,** *5* (5), 548-560.
53. Brindle, K., New approaches for imaging tumour responses to treatment. *Nat. Rev. Cancer* **2008,** *8* (2), 94-107.

54. da Silva, R. P.; Clow, K.; Brosnan, J. T.; Brosnan, M. E., Synthesis of guanidinoacetate and creatine from amino acids by rat pancreas. *Br. J. Nutr.* **2014,** *111* (4), 571-7.
55. Ide, T.; Chu, K.; Aaronson, S. A.; Lee, S. W., GAMT joins the p53 network: branching into metabolism. *Cell Cycle* **2010,** *9* (9), 1706-10.